Journal of Anatomy

J. Anat. (2019) **234**, pp419–437 doi: 10.1111/joa.12934

REVIEW ARTICLE

Challenges in creating dissectible anatomical 3D prints for surgical teaching

Ratheesraj Ratinam,[1] Michelle Quayle,[1] John Crock,[2] Michelle Lazarus,[1] Quentin Fogg[1,3] and Paul McMenamin[1]

[1]*Department of Anatomy and Developmental Biology, Centre for Human Anatomy Education, Monash University, Clayton, Vic., Australia*
[2]*Department of Surgery, Monash University, Clayton, Vic., Australia*
[3]*Department of Anatomy and Neuroscience, The University of Melbourne, Melbourne, Vic., Australia*

Abstract

Three-dimensional (3D) printing, or additive manufacturing, is now a widely used tool in pre-operative planning, surgical teaching and simulator training. However, 3D printing technology that produces models with accurate haptic feedback, biomechanics and visuals for the training surgeon is not currently available. Challenges and opportunities in creating such surgical models will be discussed in this review paper. Surgery requires proper tissue handling as well as knowledge of relevant anatomy. To prepare doctors properly, training models need to take into account the biomechanical properties of the anatomical structures that will be manipulated in any given operation. This review summarises and evaluates the current biomechanical literature as it relates to human tissues and correlates the impact of this knowledge on developing high fidelity 3D printed surgical training models. We conclude that, currently, a printer technology has not yet been developed which can replicate many of the critical qualities of human tissue. Advances in 3D printing technology will be required to allow the printing of multi-material products to achieve the mechanical properties required.

Key words: additive manufacturing; biomechanical; multi-material; surgery; three-dimensional printing; training.

Introduction

Three-dimensional (3D) printing is now a widely used tool in pre-operative planning (Arvier et al. 1994; Berry et al. 1997; Potamianos et al. 1998; Petzold et al. 1999; Chang et al. 2003; Seitz et al. 2004; Mahaisavariya et al. 2006; Jacobs et al. 2008; Singare et al. 2009; Honiball, 2010; Giovinco et al. 2012; Krishnan et al. 2012; Tam et al. 2012; Klein et al. 2013; Zein et al. 2013; Duncan et al. 2015; Huang et al. 2015; Rose et al. 2015b), surgical teaching (Cohen & Reyes, 2015; Huang et al. 2015; Scawn et al. 2015) and simulator training (Benet et al. 2015; Ryan et al. 2015, 2016), and attitudes toward image donation for 3D printing in anatomy education as oppposed to body donation may be more favourable (Abouhashem et al. 2017). Creating multi-material 3D prints that mechanically resemble real tissues is a primary focus within these educational domains (Mori et al. 2010; Hochman et al. 2013, 2015a,b; Lipton et al. 2014; Rose et al. 2015a,b), yet models that precisely match the biomechanical and visual qualities of human tissue do not currently exist. Advances in this area require knowledge of both engineering and a familiarity with the physical and biomechanical properties of each of the various human tissues. Although the biomechanical properties of some tissues have been reported (Sunderland & Bradley, 1961a; Sunderland, 1965; Diamant et al. 1972; Mozersky et al. 1972; Mow et al. 1984; Mosler et al. 1985; McBride et al. 1988; Rydevik et al. 1990; Millesi et al. 1995; Driscoll et al. 2002; Korhonen et al. 2002; Maganaris, 2002; Lieber et al. 2003; Currey, 2004; Liebschner, 2004; Phillips et al. 2004; Imer et al. 2009; Van Loocke et al. 2009; Krasiński et al. 2010; Morrow et al. 2010; Rossmann, 2010; Holeček et al. 2011; Topp & Boyd, 2012; Alkhouli et al. 2013; Boyer et al. 2013; Matschke et al. 2013; Lackey et al. 2014; Matsuhashi et al. 2014; Ottenio et al. 2015; Ugbolue et al.

Correspondence
Ratheesraj Ratinam, Department of Anatomy and Developmental Biology, Centre for Human Anatomy Education, Monash University, 9 Kenneth St Preston, Vic. 3072, Australia. E: raf.ratinam@gmail.com

Accepted for publication *6 December 2018*
Article published online *1 February 2019*

2015), a gap exists between this knowledge and its relation to 3D print engineering. This review serves to help address this gap by providing a primer on biomechanical properties of various tissues, an overview of required 3D printing materials, and a summary of the current opportunities and challenges in creating dissectible anatomical prints. Supporting Information Appendix S1 provides definitions of key biomechanical terms (emphasised in *italics*) used throughout this paper. Three-dimensional print materials (Table 1A,B) are suggested for each of the various tissue types discussed based on biomechanical characteristics (Figs 1–7).

Progression of 3D printing technology

Three-dimensional printing, otherwise known as additive manufacturing or rapid prototyping (Gibson et al. 2014), was invented in 1984 by Charles W. Hull and was later commercialised by 3D Systems Corp. (Rockhill, SC, USA) in 1989 (Horvath, 2014). Lately the use of 3D printing has greatly expanded, including into the realm of medicine where the technology is being used to make 3D anatomical teaching models (Lim et al. 2016), develop artificial organs (Murphy & Atala, 2014) and create individualised treatment delivery devices (Weisman et al. 2015).

The American Society for Testing and Materials (ASTM) created a set of standards that classify 3D printing processes into seven categories according to standard terminology: (1) Vat Photopolymerisation, (2) Powder Bed Fusion (3), Material Extrusion (4), Material Jetting (5), Binder Jetting (6), Sheet Lamination and (7) Directed Energy Deposition. All these printers essentially print objects in a layer by layer fashion but do this in very different ways (Gibson et al. 2014). Sheet lamination and directed energy deposition are two 3D printing technologies that are unlikely to ever be suitable for creating dissectible anatomical 3D prints and will not be included in further discussion.

Qualities needed in materials to replicate properties of human tissue

Both the intracellular and extracellular environment influences the biomechanical properties of a particular tissue. Tissue properties can only be accurately replicated when the effect of the extra-cellular matrix (ECM) is considered (Holzapfel, 2001). Mechanically, the key components of the ECM include collagen, elastin and proteoglycans (PG). The specific mechanical requirements of that tissue is therefore greatly influenced by the concentrations and arrangement of these three elements (Holzapfel, 2001).

The relative amounts of collagen in each tissue type are important to consider as collagen imparts *tensile* strength and rigidity to tissues (Comninou & Yannas, 1976; Holzapfel, 2001; Raub et al. 2008). In most connective tissues, collagen fibres form a two- or three-dimensional network and this results in the *anisotropic* behaviour of some of these tissues such as skin and tendons (Comninou & Yannas, 1976). *Anisotropic* behaviour leads to a tissue having varying *tensile strengths* depending on the direction of the applied force. Hence, the *anisotropic* effect of collagen is important to consider in any attempt to replicate tissues artificially.

Elastin is an elastic insoluble protein in connective tissue (Kumbar et al. 2014) that is present as thin strands in tissues such as lung, skin and blood vessels. It can be stretched to 2.5 times its original length (Holzapfel, 2001). Skin and vascular tissues contain a high amount of elastin, whereas liver, brain, heart and kidney contain low amounts (Neuman & Logan, 1950).

Proteoglycans form a viscous lubricating matrix between collagen fibrils. They permit a shearing interaction between a layer of fibrils and a layer of matrix, resulting in *viscoelastic* behaviour of soft tissues such as *relaxation* and *creep* (Holzapfel, 2001). PGs and glycosaminoglycans (GGs) attract and bind water and are therefore essential as the medium by which most cells and tissues receive nourishment. The biochemical makeup of PGs and GAGs, together with the water content, means that soft tissues display semi-permanent, as opposed to permanent (plastic), deformation when subjected to a deforming force. This is therefore another mechanical engineering consideration for model design. This, perhaps more than anything else, may be essential for producing a life-like feel.

Challenges and limitations in replicating bodily tissues with 3D printing

Creating 3D printed models that are mechanically similar to living tissues will most likely require the replication of core tissue types + the supporting tissues, such as the extracellular matrix (ECM). Tissues also exhibit varying levels (and consistency) of fluid, both intracellular and extracellular. This is important, as deformation of tissue is accompanied by redistribution of this fluid (Holeček et al. 2011). These factors, together with the physical properties of the intracellular structural framework (actin, myosin) and extracellular matrix (calcified and non-calcified), present significant challenges for the creators of 3D printing materials. The *viscoelastic* properties of tissues (*hysteresis*, *creep* and *stress relaxation*) result from biopolymers and the presence of intracellular and extracellular fluid (Holeček et al. 2011). Multiple materials (within each tissue type) may therefore be needed when replicating particular anatomical structures, e.g. a muscle and its associated tendon will likely require more than two materials. To what extent cellular and extracellular mechanical properties should be considered in simulation of tissue-level mechanics remains to be discovered.

In addition to anatomical realism, it will be desirable in the long-term for 3D prints for surgical simulation to replicate layers/planes (Benet et al. 2015; Kurenov et al. 2015;

Table 1 Summary of challenges in replicating (A) musculoskeletal/connective and (B) neurovascular tissues with 3D print material suggestions and possible future solutions.

System	Tissue	Challenging physical qualities	Material suggestion	Possible future solutions
(A)				
Musculoskeletal/ connective tissue	Bone	Trabecular bone	Visijet PXL core (3D Systems Corp.) cured with Colorbond infiltrant (3D Systems Corp.) Accura (3D Systems Corp.) Rigid palette (Stratasys Ltd) *High flexural strength and tensile strength needed*	Using a liquid support material
	Cartilage	Lubricated surface and shock-absorbing qualities	Duraform Flex, Visijet CE-NT or CE-BK materials (3D Systems Corp.) Flex TPE (Stratasys Ltd, Minnesota, U.S.A.) *Similar elastic modulus and rubber-like flexibility/cushioning and good tear resistance*	Create a composite material with a low friction coefficient component on the surface and shock absorbing component beneath
	Muscles	Anisotropic behaviour (Morrow et al. 2010). Contracts in response to electrical currents (Wain et al. 2010)	Mixture of the Visijet CR and CE materials (3D Systems Corp.) *High tensile strength and modulus, but also high elongation till at breaking point and flexibility*	Incorporating the fibre oriented structure of muscle into a 3D print. Use of stimuli responsive hydrogels (Tanaka et al. 1982)
	Tendons	Physical properties vary according to shape of tendon and tendon location	Visijet SL Proflex material (3D Systems Corp.) Rigur +Tangoplus (Stratasys Ltd) *Tensile strength* and flexibility to mimic tendon tissue	Each tendon in the human body would need to be tested for its individual strain characteristics
	Ligaments	Tri-phasic strain behaviour	Duraform Flex (3D Systems Corp.) Flexibility, low *tensile strength* and *elastic modulus*	Replicate collagen fibrils on a macroscopic level
	Aponeuroses	High tensile strength and modulus of elasticity	Visijet SL Proflex material (3D Systems Corp.) *Tensile strength* and flexibility	Use of high strength flexible material such as silicon
	Skin	Anisotropy and tension lines throughout human body	Mixture of Visijet CE and CR materials (3D Systems Corp.) *Tensile strength* and elastomeric properties	Induce tension in skin layer of print post-printing
	Adipose tissue	Extensive collagenous ECM and difference in properties depending on anatomical location	Visijet CE-NT/CE-BK or Duraform Flex material (3D Systems Corp.) Flex TPE material (Stratasys Ltd) *Low tensile strength and elastic moduli, cushioning properties*	Individual testing of adipose tissue in all areas of the human body. Use of multimodal printing to mimic fatty tissue being printed within a collagenous ECM

(continued)

Table 1. (continued)

System	Tissue	Challenging physical qualities	Material suggestion	Possible future solutions
B) Neurovascular	Nerves	Conductive qualities	Duraform Flex (3D Systems Corp.) Elastomeric rubber like properties. Similar tensile elongation at break, and low *elastic modulus* and *tensile strength*	Use of pressure sensing materials (Pan et al. 2014)
	Arteries	Three layered hollow structure and different properties depending on anatomical location	Visijet CE materials (3D Systems Corp.) Elastomeric properties and their low tensile strength and elastic moduli	Use of a multimodal printer that uses a liquid support material that can easily be removed. Varying material selection depending on anatomical location of vessel
	Veins	Three-layered hollow structure and different properties depending on anatomical location. Blood needing to flow from arterial system to venous system	Visijet CE materials (3D Systems Corp.) Low *elastic moduli* and elastomeric properties	Use of a multimodal printer that uses a liquid support material. Obliterate capillary network. Artificially create connections between arterial and venous system or have separate circulations for each

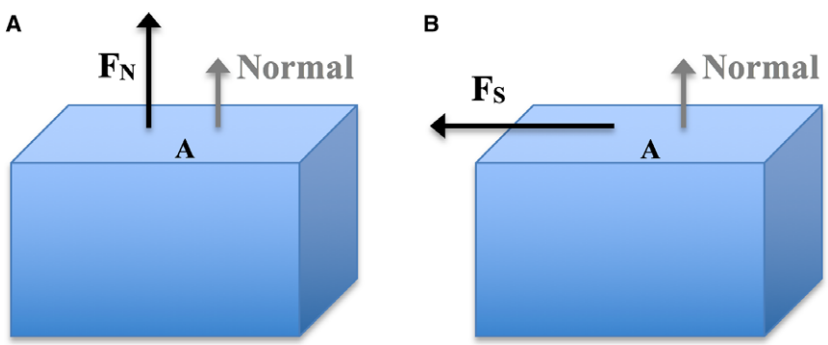

Fig. 1 Object subjected to uniaxial normal stress and shear stress. The direction of the normal is indicated in grey (perpendicular to surface 'A'). (A) Normal force F_N acting on surface 'A' of object results in a normal stress. (B) Shear force F_S acting across surface 'A' of object, results in a shear stress.

Mowry et al. 2015; Ryan et al. 2015, 2016; Schmauss et al. 2015; Souzaki et al. 2015; Olivieri et al. 2016; Tai et al. 2016; Vakharia et al. 2016). Surgeons often operate along tissue planes to minimise trauma, as suggested by the quip: 'intimate knowledge of the correct plane distinguishes the master from the pedestrian surgeon' (Kirk, 2010). Tissue planes can be subtle and can be indicated by (1) a particular anatomical landmark, e.g. 'white line of Toldt' is identified before mobilisation of a section of colon during colectomies (Pigazzi et al. 2007); (2) subtle colour differences between adjacent tissues, e.g. identifying the gallbladder and transverse colon during a cholecystectomy; and (3) areolar connective tissue spreading apart between two separable adjacent structures on application of a tensile force, e.g. dissecting the gallbladder from the liver during a cholecystectomy. These different structures would need to have specific physical properties that would allow for planar dissection.

Tissue response to surgical insults may also need to be considered if true realism is the objective, e.g. vasospasm of

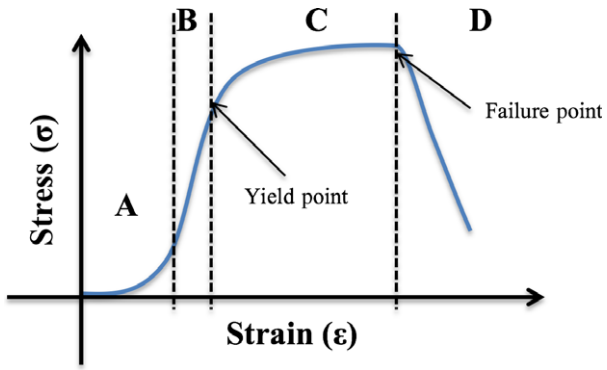

Fig. 2 Example of stress–strain curve for soft tissue adapted from Korhonen & Saarakkala (2011). (A) Initial toe region, with straightening of collagen fibrils and non-linear stress–strain relationship. (B) Elastic region of stress–strain curve where stress is linearly proportional to strain. The slope of this region is equal to Young's modulus of the tissue. All changes are reversible in this region. (C) Plastic region: the yield point is at the start of this region and permanent deformation occurs beyond this point. (D) At the end of the plastic region, sudden failure of the tissue occurs (the failure point) and the stress dissipates.

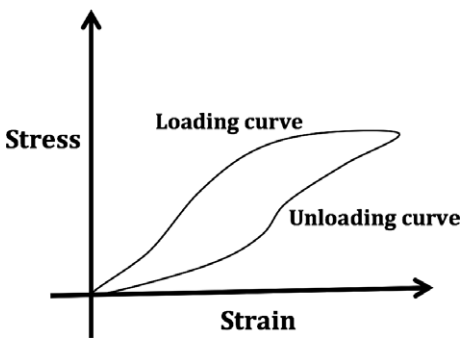

Fig. 3 Hysteresis loop.

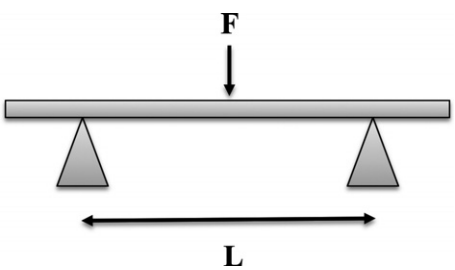

Fig. 4 Typical 3-point bending test with force applied to beam.

arteries when transected, contraction of muscle cells in response to diathermy, drug-induced changes (abdominal wall tension changes due to anaesthetic) and dynamic operating fields (pneumoperitoneum with carbon dioxide). Thus, one limitation of current 3D prints is that they would not react accurately to surgical trauma. Having materials that can safely undergo diathermy and not release toxic fumes upon doing so, is also of critical importance given the popularity and frequency of its use among surgeons (Lam, 1985; Saran et al. 1994; Segal et al. 1997; Sengupta & Webb, 2001; Stenquist et al. 2002; Ussmueller et al. 2004). Whether this can be achieved is at present unknown.

Three-dimensional prints that accurately replicate the physical properties of human tissue can be seen in the area of scaffold engineering, where 3D printing provides a wide array of materials in powdered form and offers much flexibility with regard to geometrical options. This is due to its use of additive rather than subtractive methods in producing a finished product (Butscher et al. 2011). In particular, the use of hydrogels in making scaffolds could be applied to dissectible 3D models. Tissue-engineering techniques depend on utilising material scaffolds, which serve as a synthetic extracellular matrix (Drury & Mooney, 2003). Poly(lactide-co-glycolide) (PLG) is an example of a hydrogel that is mechanically strong and has been approved by the Federal Drug Administration (FDA) for use within humans. Due to their ability to absorb a large volume of water, hydrogels are better able to mimic soft tissue and can retain a significant fraction (> 20%) of water within their structure without dissolving in the water (Ratner & Hoffman, 1976). A 3D printing process that incorporates hydrogel material into its printing process could result in prints that more closely resemble body tissues, although their degradable nature would mean that they may be single-use only.

Three-dimensional printing uses a variety of raw materials such as plastics, resins, super alloys, stainless steel, titanium, polymers and ceramics (Berman, 2012; Gibson et al. 2014). The materials used in 3D printing (Table 2A,B) are rapidly expanding, as is their potential in multi-material 3D printing. Materials clearly not suitable for replicating bodily tissue characteristics include the super alloys, steel and titanium. Materials that show some potential include the SLA Accura and Selective Laser Sintering (SLS) range (3D Systems Corp.) and Fused Deposition Modelling (FDM) range (Stratasys Ltd, Eden Prairie, MN, USA). Though these materials are designed for durable industrial grade parts (ABS-like, Polypropylene-like, Durable and Clear class materials) and are printed for 'snap-fit', they could serve some role in replacing bony structures due to their high level of flexural strength. Three-dimensional printers with multi-modal printing abilities include the Visijet Elastomer materials on the Projet 5500X printer (3D Systems Corp.) and the Polyjet materials (Stratasys Ltd). Prints made with Polyjet printers (Stratasys Ltd) can have up to 360 000 colours, a high resolution of 100 μm and varying levels of flexibility, toughness, durability and translucency. A print resolution of 100 μm is necessary in certain medical areas, such as 3D printing of fractured bones; here a 2000-μm step-off in the articular surface of a joint can determine whether a surgeon will operate (Knirk & Jupiter, 1986; Bradway et al. 1989). Although these options, together with the use of an increasing number of print heads to increase speed of production, make this a viable option when making anatomical models, there

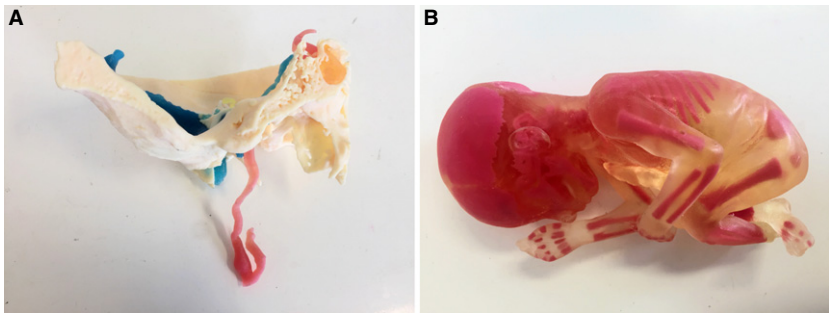

Fig. 5 Multi-material prints (Centre for Human Anatomy Education) created using the Stratasys 'J750' Multi-material 3D printer (Stratasys Ltd). (A) Base of skull showing path of internal carotid artery and sigmoid sinus/internal jugular vein (superior bulb). (B) Multi-material print of fetus.

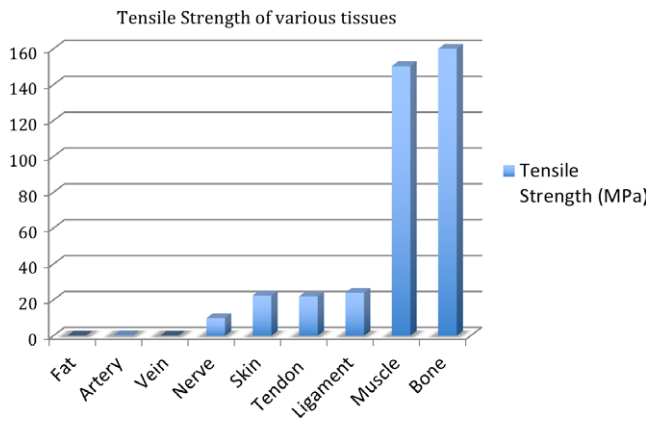

Fig. 6 Comparison of the tensile strength of various body tissues.

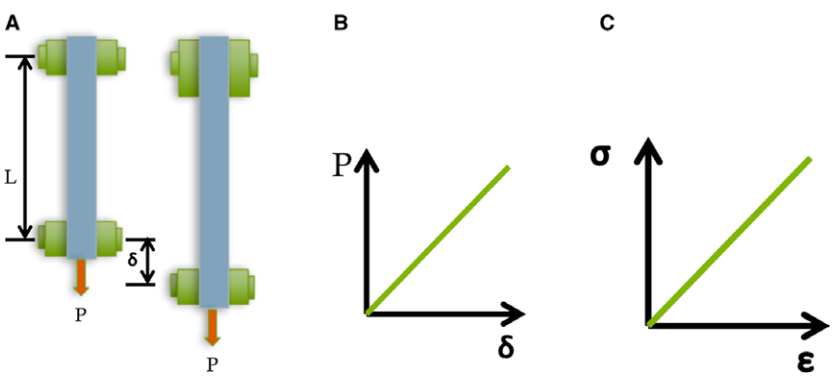

Fig. 7 Tensile test adapted from Lardner (1994). (A) The test specimen (blue) is subjected to a uniaxial force 'P'. This results in displacement δ. (B) For each value of 'P', the value for δ can be measured and plotted to form a load-displacement curve. This curve is linear for linear-elastic materials (Lardner, 1994). (C) The force 'P' gives rise to uniform axial stress σ which equals 'P' divided by 'A', where 'A' is the cross-sectional area of the specimen. The normal strain ε is given by δ divided by the original length of the specimen. The slope of this stress–strain curve equals the Young's modulus for the material, denoted by 'E'.

is still a lack of empirical evidence about their use to create medical implantable devices or surgical simulation models.

A recent addition to the FDM range is the PORO-LAY range of filaments (CC-Products, Cologne, Germany). These filaments include Lay-Felt, Lay-Tekkks, Lay-Fomm and Gel-Lay (Pei, 2014). These materials are highly porous foam-like elastomeric polymers that are initially 3D-printed as a composite of hard and soft material (Melnikova et al. 2014). Post-processing with warm water removes the hard component, leaving a soft porous material (Melnikova et al. 2014), to which various infiltrates can be added to give different mechanical properties.

FDM printers generally work with different types of ABS, PC and Nylon with the aim to produce materials that are

Table 2 (A) Properties of 3D print materials made by 3D Systems Corp. As a comparison, human tissues range from a tensile strength of 13.7 MPa (fat) to 165.77 MPa (bone). (B) Properties of 3D printing materials provided by Stratasys Ltd. As a comparison, human tissues range from a tensile strength of 13.7 MPa (fat) to 165.77 MPa (bone).

Units	Tensile strength MPa	Tensile modulus MPa	Tensile elongation at breaking point %	Flexural strength MPa	Flexural modulus MPa	Physical properties MPa
(A) 3D Print Material Properties : 3D Systems Corp. (3D Systems Corp., 2017a)						
SLA materials						
Accura 25	58	1590–1660	13–20	55–58	1380–1660	Snap-fit. Rigid. Opaque white. Flexible with shape retention. For master patterns for silicon molding
Accura Amethyst	22–38	3514–3996	0.56–1.04	87–125	3652–3721	Fine detail models. Used in jewelry design
Accura Peak	57–78	4220–4790	1.3–2.5	77–126	4180–4790	High stiffness. Moisture, thermal resistance. High accuracy
Accura Ceramax Composite	78–87	9460–9680	1.0–1.5	137–145	8270–8370	Rigid ceramic composite. Highest stiffness in SLA range. Thermal, moisture, abrasion resistant
Visijet PXL colorbond	14.2	9450	0.23	31.1	7163	Colour vibrancy. Quick-cure
Visijet PXL Strength Max	26.4	12560	0.21	44.1	10680	Strength. Ideal for functional models
Visijet PXL – Wax	9.2	22570	0.09	11.7	4833	Fast, colour models. Strong. Smooth surface
Visijet M3 (MJP)	32–49	735–2168	6.1–19.7	26.6–65	–	Stiff. High thermal resistance. For precision dental moulds
Visijet SL Flex	38	1620	16	57	1420	Tough. Snap-fit assemblies. Flexible. Master patterns for vacuum casting
Visijet Proflex	15–20	250–350	65–75	N/A	N/A	Flexible, transparent, clear.
Visijet CR-WT	37–47	1000–1600	7–16	61–72	1400–2000	High rigidity and durability. Can mix with another Visijet CR/CE material to form composite materials
Visijet CR-CL	37–47	1000–1600	7–16	61–72	1400–2000	Rigid. Can mix with another Visijet CR/CE material to form composites
Visijet CE-NT	0.2–0.4	0.27–0.43	160–230	N/A	N/A	Elastomeric. Can mix with another Visijet CR/CE material to form composites
Visijet CE-BK	0.2–0.4	0.27–0.43	160–230	N/A	N/A	Elastomeric. Mix with another Visijet CR/CE material to form composites
SLS materials						
Duraform Flex	1.8	7.4	110	–	4.9	Elastomer. Rubber-like flexibility. Durable. Good tear resistance
Duraform GF	26	4068	1.4	37	3106	High stiffness. Thermal resistance. Autoclave compatible.
(B) 3D Print Material Properties: Stratasys Ltd (Stratasys Ltd., 2014, 2017b,c)						
FDM materials						
ABSplus-P430	33	2200	6	35–58	1650–2100	Smooth, durable
PC-ABS	41	1900	6	68	1900	Strong, heat-resistant
PC	42–57	1944–1958	2.5	68–89	1800–2006	Durable, stable
Nylon 12	38.5–46	1138–1282	5.4–30	61–67	1180–1276	Snap-fit. High fatigue, chemical resistance

(continued)

Table 2. (continued)

Units	Tensile strength MPa	Tensile modulus MPa	Tensile elongation at breaking point %	Flexural strength MPa	Flexural modulus MPa	Physical properties MPa
Stereolithography materials						
Somos Watershed XC11122	50.4	2770	15.5	68.7	2205	Strong, tough, water-resistant. Nearly colourless.
SC 1000P	53	2668	4–8	83	1930	Low deformation due to shrinkage. For investment cast industries and models with highly involved geometries
Laser sintering materials						
Nylon 12CF	51–60	2461–3654	5.3–5.7	70–113	2482–6067	Carbon fibre-filled. High thermal and wear resistance. High stiffness and tensile strength
Nylon 12 HST	31–48	2900–5500	2.7–4.5	65–85	2688–4412	High stiffness, non-conductive, transparent. Thermal resistance
Nylon 11 FR	39–46	1448–1586	21–38	54–55	1517–1551	Polyamide. Fire-resistant. High elongation at breaking point
Flex TPE (Thermo-plastic elastomer)	–	8	110	–	3–23	Soft, extreme elongations possible. Cushioning applications. High ductility
PolyJet materials						
Rigid opaque materials						
Veroblue RGD840	50–60	2000–3000	15–25	60–70	1900–2500	Rigid. High detail parts.
Vero Purewhite RGD837	50–65	2000–3000	10–25	75–110	2200–3200	Rigid. High detail parts
Transparent material						
VeroClear RGD810	50–65	2000–3000	10–25	75–110	2200–3200	Transparent.
Simulated polypropylene materials						
Duruswhite RGD430	20–30	1000–1200	40–50%	30–40	1200–1600	Tough, flexible, durable
Rigur RGD450	40–45	1700–2100	20–35%	52–59	1500–1700	Tough, durable. White. Snap-fit

MPa, megapascal.

biocompatible, translucent, high in tensile and/or flexural strength, tough, or are resistant to heat or chemicals. With these materials, FDM technology appears geared more for medical devices rather than surgical/anatomical models.

Tissue-specific challenges

Biomechanical data, namely *tensile/compressive strength* and *elastic modulus*, were collected for various bodily tissues from the literature. Mechanical properties for 3D printing materials provided by two large 3D printing companies, are also presented as a comparison. Whereas not exhaustive, this review does demonstrate the extensive range of materials available.

Three-dimensional printing of bone

Cortical bone composition and structure can vary significantly and thus greatly influence the tissue mechanical properties (Li et al. 2013). From a mechanical perspective, the architecture of bone has a hierarchical organisation whereby each level contributes distinct qualities to mechanical properties measured (Table 3): (1) a whole bone level; (2) an architectural level, which refers to the volumes of cortical or trabecular bone tissue; (3) a tissue level, containing single trabeculae, single osteons and cortical microbeams; (4) a lamellar level; and (5) an ultrastructural level containing isolated molecular and mineral components of the bone (Liebschner, 2004).

A challenge in replicating bone as a 3D print for surgical teaching purposes is to mimic trabecular or cancellous bone. Integrating a fluid component into miniscule compartments in a 3D print, to mimic the structure of either red or yellow marrow, is a challenge yet to be overcome by current 3D printing technology. Copying the mechanical properties of bone would mean trying to replicate the hierarchical organisation; this will require a method for printing density non-homogeneously, a difficulty not easily overcome with current print technology. Anatomical site-specific differences in bone properties may also have to be considered. An exemplar of this would be replication of temporal bone.

Table 3 Biophysical properties of bone.

System: Musculoskeletal/connective tissue						
Tissue: Bone						
	Mild osteogenesis imperfecta (Albert et al. 2013)	Severe osteogenesis imperfecta (Albert et al. 2013)	Bovine Femur (Albert et al. 2013)	Femur 35-year-old male (Currey, 2004)	Femur 5-year-old male (Currey, 2004)	Femur 3-year-old male (Currey, 2004)
Young's modulus, MPa	4500	5100	16 100	16 700	12 800	7000
Flexural strength, MPa	94	74	251	–	–	–
Yield Strength/stress, MPa	65	57	180	122.3	76.9	98.0
Yield strain	0.0166	0.0143	0.0136	0.00723	0.0102	0.0088
Post yield strain	–	–	–	0.02202	0.0431	0.03427
Post yield stress, MPa	–	–	–	43.4	46.4	46.8
Ultimate tensile strength, MPa	–	–	–	165.7	123.3	144.8

MJ: megajoule; MPa: megapascal.

Table 4 Biophysical properties of cartilage.

System: Musculoskeletal/connective tissue								
Tissue: Cartilage								
	Degenerative Grade 3* (Hori & Mockros, 1976)	Degenerative Grade 2* (Hori & Mockros, 1976)	Degenerative Grade 1* (Hori & Mockros, 1976)	Grade N* (Hori & Mockros, 1976)	Bovine Humeral (Korhonen et al. 2002)	Bovine Patellar (Korhonen et al. 2002)	Bovine Femoral (Korhonen et al. 2002)	Bovine Calf (Bursać et al. 1999)
Shear modulus, MPa	0.62	1.24	3.29	1.66	–	–	–	–
Bulk modulus, MPa	1.94	0.95	1.90	3.40	–	–	–	–
Young's modulus, MPa	1.84	3.56	9.33	4.91	0.8 ± 0.33	0.57 ± 0.17	0.31 ± 0.18	1.50 ± 0.50
Poisson's ratio	0.48	0.44	0.42	0.48	0.15 ± 0.06	0.16 ± 0.05	0.21 ± 0.05	

*Bollet classification (Bollet et al. 1963). Indicates degree of cartilage erosion. Grade N: Normal, cartilage is smooth, white, glistening and firm. Grade 1: Earliest lesions, minimal pitting and fraying of the surface. Grade 2: Obvious irregularity of cartilage surface with pitting and fraying, some softening but normal thickness. Grade 3: Extensive fraying and irregularity of surface, marked softening and some thinning of the cartilage.

Current polyurethane bone mimics such as 'Sawbones' (Sawbones, Pacific Research Laboratories, Vashon, WA, USA) and 'SYNBONE' (SYNBONE, Graubünden, Switzerland) are commonly used in orthopaedic training and in the mechanical analysis of orthopaedic constructs (Flahiff et al. 1995; Khuri et al. 2003; Poole et al. 2016). These mass-produced products have been engineered to replicate the generic biomechanical properties of bone but do not allow individual users to 3D-print bones using their own 3D data. 'SYNBONE' uses a variety of traditional manufacturing techniques together with 3D printed moulds to create their products, providing a generic bone-like material (SYNBONE 2017).

Three-dimensional printing of cartilage

Articular cartilage is a highly specialised, thin, avascular layer of connective tissue that overlies the articulating bony

Table 5 Biomechanical properties of ligament, muscle, tendon and aponeuroses.

System: Musculoskeletal/connective tissue					
Tissue: Muscle/tendon/ligaments/aponeuroses					
	Human muscle (Lieber et al. 2003)	White rabbit extensor digitorum muscle – longitudinal extension* (Morrow et al. 2010)	White rabbit extensor digitorum muscle – transverse extension* (Morrow et al. 2010)	Palmaris longus tendon (Millesi et al. 1995) (SEM)	Human cadaver supraspinatus tendon – anterior sub-region (Matsuhashi et al. 2014)
Young's modulus, MPa	462.5 ± 99.6 (muscle fibre bundle) 111.2 ± 35.5 (Individual sarcomere)	0.447 ± 0.098	0.022 ± 0.015	–	592.4 ± 237.4
Tensile strength, MPa	150.4 ± 25.7	0.447 ± 0.097	0.022 ± 0.015	–	22.1 ± 5.4
Hysteresis loop	–	–	–	0.079 (0.005)	–
Residual strain	–	–	–	0.0023 (0.005)	–
Ultimate failure load, Newtons	–	–	–	–	779.2 ± 218.9
Elongation at breaking point, %	–	50.5 ± 22.2	182 ± 92.4	–	–

SD, standard deviation; SEM, standard error of mean.
1 MPa = 1 × 10^6 Newton per square metre.
*Skeletal muscle dissected free from aponeuroses.

ends of joints. It not only lowers friction but also allows for efficient load bearing. Cartilage is formed by chondrocytes that are embedded in a highly hydrated and organised extracellular matrix (ECM) consisting of Type II collagen fibres and proteoglycans. The combination of fluid and ECM imparts certain viscoelastic and mechanical properties. At mechanical equilibrium, articular cartilage is usually characterised as an isotropic elastic material with no interstitial fluid flow. Furthermore, the *elastic modulus* of cartilage actually varies in different locations within the body (Korhonen et al. 2002). Cartilage has quite a small *Young's modulus*, meaning minimal stress would create strain (Table 4).

The difficulty in replicating cartilage as a 3D print would be in creating a material that will (1) imitate the lubricating properties of cartilage, (2) adhere firmly to the surface of the 3D printed bone without shearing and (3) possess the same *viscoelastic* properties of cartilage. This challenge could probably be tackled not only by creating a 3D printed material with a high amount of water incorporated into it, to replicate the *viscoelastic* properties of cartilage, but also by creating a print with a low enough static and kinetic frictional component to allow the same ease of movement of joints in a 3D print. The current high-end printers such as the Stratasys 'Connex 3 Objet260' (Stratasys Ltd) series and 3D systems 'Projet 3500' (3D Systems Corp.) series can both print at a layer resolution of 16 μm, allowing for the creation of very smooth surfaces (3D Systems Corp. 2017b, Stratasys Ltd. 2017a). This would most likely require a composite material to be used; one in which the surface material provides the low friction coefficient and the deeper component the shock-absorbing qualities. Interfacing with adjacent printed material replicating bone will require careful consideration if separation at interfaces is to be avoided.

Three-dimensional printing of muscle

The tensile properties of muscle tissue are influenced by both individual muscle cells and the ECM. The latter is critical for stabilising groups of muscle cells within muscle fibre bundles. The ECM represents a dynamic component of normal muscle tissue and, even though only a small amount of muscle tissue is ECM, it contributes greatly to muscle *tensile strength*, its *tensile modulus* being over 300 times that of muscle cells (Lieber et al. 2003). Skeletal muscle is composed of about 70–80% water, 3% fat and 10% collagen (Vignos & Lefkowitz, 1959; Van Loocke et al. 2009). The composition and fibre-oriented structure of muscle, together with the orientation of the collagenous 'sheaths' at the endomysium, perimysium and epimysium levels, give muscle *anisotropic* elasticity and *viscoelastic* behaviour (Van Loocke

Human cadaver supraspinatus tendon – posterior sub-region (Matsuhashi et al. 2014)	Human patellar tendon – Healthy controls (Matschke et al. 2013) (SEM)	Human patellar tendon – rheumatoid arthritis (Matschke et al. 2013) (SEM)	Transverse carpal ligament (Ugbolue et al. 2015) (SD)	Vertebral aponeuroses (Loukas et al. 2008) (SD)	Palmar aponeuroses (Millesi et al. 1995) (SEM)	Gastrocnemius aponeuroses (Azizi et al. 2009) (SD)
217.7 ± 102.1	740 (80) 900 (10)	590 (70)	–	–	–	744.4 (219) 115.7 (67)
11.6 ± 5.3	–	–	23.99 (10.7)	–	–	53.2 (12.9) 28.1 (8.7)
–	–	–	–	–	0.086 (0.008)	–
–	–	–	–	–	0.0016 (0.0003)	–
335.6 ± 164.0	–	–	–	38.7 (6.8)	–	–
–	–	–	28	–	–	–

et al. 2009). With the aponeurosis or tendon intact, the linear *moduli* are significantly higher (Morrow et al. 2010). With the aponeuroses (or tendon) removed, skeletal muscle still has a significantly higher *elastic modulus* in the fibre direction than in the cross-fibre direction (Morrow et al. 2010). Muscle has a high *tensile strength* (*ultimate stress*) value parallel to muscle fibres and a relatively low *tensile strength* transversely (Table 5).

The *anisotropic* quality of muscle, its fibre-oriented structure or fascicular pattern, and its supportive collagenous matrix would need to be incorporated on some level in a 3D print. Three-dimensional prints are inherently anisotropic due to their layer-by-layer formation. Muscle tissue also contracts when subjected to a current/diathermy (LaCourse et al. 1988; Wain et al. 2010). A material that could be safely electro-cauterised and contract in response to the electrical current would be difficult to simulate. Stimuli-responsive hydrogels might be a possible future solution. They are active materials capable of changing their properties, such as volume, reversibly in response to changes in the energy-based conditions of their liquid (e.g. electric fields or light) (Tanaka et al. 1982; Richter, 2009). Soft robotics could provide the answer with 3D-printed McKibben-style artificial muscles (Sangian et al. 2018) or 3D-printed, electrically driven, soft actuator material artificial muscles (Aslan et al. 2017). Whether these materials could reliably and affordably be integrated into 3D prints remains to be seen.

Three-dimensional printing of tendons, ligaments and aponeuroses

The role of tendons is to transmit contractile forces from muscles to the skeleton. Tendon is a uniaxial structure of mainly parallel type I collagen fibrils and elastin embedded in a proteoglycan-water matrix. Collagen accounts for 65–80% of the dry mass of the tendon and elastin approximately 1–2%. Tendons respond to stress by initial straightening of their wavy fibres. Tendons do not behave like rigid structures and instead display *viscoelastic* properties (Maganaris, 2002). The collagen within tendons is the most important factor for the mechanical strength of a tendon (McBride et al. 1988). The mechanical and morphological properties of connective tissues such as tendons and ligaments vary according to their level of mechanical stimulation. The overall shape of a tendon can greatly impact the *modulus of elasticity* and ultimate failure loads (Matsuhashi et al. 2014). This is seen in the case of the supraspinatus tendon and its anterior and posterior sub-regions. Being thicker and tubular, the anterior sub-region was found to have a higher *ultimate stress* and *modulus of elasticity* compared with its posterior region counterpart, which is thinner

and strap-like, at least in human cadaveric specimens (Matsuhashi et al. 2014). Human tendons and aponeuroses also reveal low values of *residual strain* and a normalised *hysteresis loop* as regard *viscoelastic* behaviour (Millesi et al. 1995), meaning there is minimal residual deformation with application of any tensile forces. Aponeuroses, a form of flattened tendon, are composed of collagen fibres which are the main load-bearing element, with thin, scattered, flexible elastin fibres forming highly branching networks between bundles of collagen that, together with proteoglycans, contribute to the viscous *stress* component (Millesi et al. 1995).

Ligaments contain dense, highly organised tissue made of collagens (Types I, III and V), elastin, proteoglycans, water and cells. Ligaments display tri-phasic behaviour when undergoing *strain* (Laurencin & Freeman, 2005). The first phase displays a low amount of *stress* per unit *strain* and is called the non-linear or toe region. The second phase shows an increase in stress per unit strain and is known as the linear region. The last phase then displays a decrease in *stress* per unit *strain* and represents the failure of the ligament. This is the *yield* and failure region (Laurencin & Freeman, 2005). The arrangement of the components of ligament tissue leads to this phenomenon. The initial application of force leads to lateral contraction of collagen fibrils, straightening of the crimp pattern and release of water (Laurencin & Freeman, 2005). After straightening of the crimp pattern, force is then transmitted to the collagen molecules, whereby the collagen triple helix is stretched and interfibrillar slippage occurs between crosslinks (Laurencin & Freeman, 2005). This is followed by fibril defibrillation during the *yield* and failure phase (Laurencin & Freeman, 2005).

Of all the tissues, human tendon, even though it possesses viscoelasticity, would be the least challenging to replicate given its low value of residual strain and normalised *hysteresis* loop. The difficulty would come in replicating different tendons, as the shape of a particular tendon greatly impacts its *modulus of elasticity* and failure load (Matsuhashi et al. 2014). Though the *tensile strength* required to mimic ligament tissue is attainable with many 3D print materials (Tables 1 and 4), it would be difficult to replicate their tri-phasic behaviour in response to *stress*. Also their properties are highly governed by the nature of their attachments (some moveable, some not). Replicating inter-fibrillar slippage and defibrillation of fibrils in a 3D print could probably only happen at a macroscopic level by incorporating fibrils into the 3D printing process, a feature not currently available. Aponeuroses would be challenging to replicate in 3D prints given their very high *tensile strength* and *modulus of elasticity*. There would be additional challenges in mimicking the manner in which these structures integrate with their bony attachments. Experience suggests this will be difficult with present technology.

Three-dimensional printing of adipose tissue

Adipose tissue is a loose vascular connective tissue primarily containing adipocytes embedded in an extensive, collagenous ECM (Ahima & Flier, 2000). Adipose tissue displays non-linear *stress–strain* behaviour in both human and animal studies (Alkhouli et al. 2013). Additionally, the biomechanical properties of human adipose tissue appear to differ depending on anatomical location. For example, human omental white adipose tissue (WAT), found in the abdomen, displays much higher *tensile strength* compared with subcutaneous WAT, probably related to the fact that subcutaneous WAT may require more malleability to accommodate energy storage and adipocyte hypertrophy (Lackey et al. 2014) (Table 6).

Even though the physical characteristics of adipose tissue vary depending on anatomical location, it would probably be less difficult to replicate as a 3D print given this tissue's simplicity in structure and function: the main difficulty would be mimicking the semifluid-like status at body temperature and the extensive collagenous ECM that supports the fat-laden adipocytes.

Three-dimensional printing of skin

Skin is the largest organ of the human body, with an area of about 1.8 m^2 and average thickness of about 2 mm. Human skin is subject to a variety of stresses whereby it is stretched, sheared and pinched, and due to its elastic properties skin tends to return to its original state following most deforming forces (Ottenio et al. 2015). The elastic properties of skin also determine the direction of the tensile force being applied in relation to tension (Langer's) lines, which reflects the underlying orientation of the majority of the collagen bundles in the dermis (Ottenio et al. 2015). Many techniques have been used to measure the mechanical properties of skin, including suction, indentation, torsion and tension tests (Sanders, 1973; Alexander & Cook, 1977; Diridollou et al. 2000; Boyer et al. 2013; Mayrovitz et al. 2017). Skin is composed of three layers – the hypodermis, dermis and epidermis. From a biomechanical standpoint skin is very complex and heterogeneous, as it displays *viscoelasticity*, is *anisotropic* and is an adhesive material showing a non-linear *stress–strain* relationship (Boyer et al. 2013). The *tensile strength* and *Young's modulus* of skin are almost double when parallel to Langer's lines (Table 6).

The most difficult challenge in replicating skin comes with mimicking Langer's lines. Pre-existing tension in skin would be difficult to incorporate into a 3D print, as 3D print materials are not under tension when printed. This challenge could possibly be addressed by adding tension into the print in the post-printing phase by creating stretch in the skin layer of the print, and possibly applying this to the print later in a more conventional manner as part of a post-production process.

Table 6 Biomechanical properties of adipose tissue and skin.

System: Musculoskeletal/connective tissue								
Tissue: Fat/skin								
	Omental fat (Alkhouli et al. 2013) (SD)	Subcutaneous fat (Alkhouli et al. 2013) (SD)	Omental fat – healthy obese women (Lackey et al. 2014) (SEM)	Subcutaneous white adipose tissue – healthy obese women (Lackey et al. 2014) (SEM)	Retroperitoneal white adipose tissue – mice (Lackey et al. 2014) (SEM)	Skin – parallel to Langer's lines (Ottenio et al. 2015) (SD)	Skin - at 45 degrees to Langer's lines (Ottenio et al. 2015) (SD)	Skin -perpendicular to Langer's lines (Ottenio et al. 2015) (SD)
Tensile strength, KPa	–	–	34.7 ± (4.2)	13.7 (2.5)	10.43 (2.49)	28 000 (5700)	22 500 (8200)	15 600 (5200)
Young's modulus, KPa	1.6 (0.8)	2.9 (1.5)	–	–	–	160 800 (53 200)	12 1000 (58 400)	70 600 (59 500)

KPa, kilopascal; SD, standard deviation; SEM, standard error of mean.

Three-dimensional printing of neurovascular structures

The structurally important materials constituting arterial walls are elastin and collagen. Though collagen has a much higher *Young's modulus* than elastin, it appears that elastin accounts for most of the elastic properties of arteries (Mozersky et al. 1972). The quantity of elastin and collagen in arterial walls varies little with age; however, there is fragmentation of elastin fibres over time, leading to more of the load being sustained by collagen fibres and thus increased stiffness (Mozersky et al. 1972). Compliance of arteries is governed by the relationship between transmural pressure and vessel diameter. In contrast to veins, arteries have a steep pressure/volume relationship indicative of less compliant vessels (McVeigh et al. 2007). Compliance depends on both the original shape and the individual components of the arterial wall, namely, smooth muscle, collagen and elastin (McVeigh et al. 2007). Together these components and their individual physical properties result in a non-linear relationship between pressure and volume. The non-linearity adds a lot of complexity and means no single number can be used to define the compliance characteristics of any blood vessel or any vascular bed (McVeigh et al. 2007). Added to this is the fact that atherosclerosis, in its fully developed form, leads to structural changes in all layers of the arterial wall, producing alterations in the *viscoelastic* properties (Mozersky et al. 1972). Reproduction of such variations may be beyond the limits of 3D printing technology for some time. Each of the layers of an artery imparts physical characteristics to it. Creating a 3D print that would mimic an artery for vascular surgery purposes might mean recreating this organisation. Difficulty would arise in smaller vessels whereby the printer would have to have a high enough fidelity to print a 3-layered tube that is also hollow and has no support material incorporated into it to allow some form of fluid to be infused into the lumen. This problem could possibly be overcome by having a liquid or water-soluble support material that can be flushed out of the print.

Compared with arteries, veins are more compliant and subject to lower pressures (Rossmann, 2010). Veins have thinner walls than arteries, which contain less smooth muscle and elastin. Though veins have a larger amount of inextensible collagen they are more distensible (Rossmann, 2010). Non-linear and *viscoelastic* behaviour is observed with veins and, adding to venous structural complexity, the microstructure and mechanical properties of veins vary with their anatomical location, position in the vascular hierarchy and stress state (Rossmann, 2010). The composition of various elastic components such as elastin and collagen influence the biomechanical characteristics of veins (Krasiński et al. 2010). The amount of collagen I and IV present in the walls of veins differs between competent and incompetent vessels, with competent human saphenous veins showing a larger amount of collagen IV, and incompetent veins displaying a greater amount of collagen I and elastin leading to a greater stiffness (Krasiński et al. 2010). The challenges in replicating veins would be similar to that of arteries given their similar structure. Replicating the artery-capillary-vein interface would also pose a challenge in terms of size and resolution of printers and the images upon which they are based. Most conventional clinical radiographic images have a resolution of approximately 130–300 μm for CT and 600 μm for MRI, whereas for micro-CT and high resolution MRI, this decreases to 8.2 and 37 μm, respectively (Kobayashi et al. 2004; Hopper, 2005; Burghardt et al. 2011). This hurdle would most likely be overcome either by artificially

Table 7 Biomechanical properties of neurovascular structures.

System: Neurovascular structures								
Tissue: Arteries/veins/nerves								
	Human femoral artery – under age 35 years (Mozersky et al. 1972) (SEM)	Human arteries – age 35–60 years (Mozersky et al. 1972; Vorp et al. 2003) (SD)	Human arteries – elderly patients (Mozersky et al. 1972; Claes et al. 2010) (SD)	Umbilical cord vein (Li et al. 2006)	Ulnar nerve (Sunderland & Bradley, 1961b; Ma et al. 2013)	Median nerve (Sunderland & Bradley, 1961b)	Rabbit Tibial Nerve (Rydevik et al. 1990)	Spinal nerve roots (Sunderland & Bradley, 1961b)
Modulus of elasticity, Mpa	0.26 (0.03)	0.388 (0.04)	0.628 (0.1)	0.03–0.06	0.01 0.05	–	–	–
Tensile strength, Mpa	–	1.71 (0.14) 1.80 (0.24)	0.39 (0.07)	–	9.8–18.6	9.8–17.7	11.7 ± 0.7	3.9–29.4
Elongation at breaking point, %	–	–	–	–	11–21	12–20	38.5 ± 2.0	

SD, standard deviation; SEM, standard error of mean.

creating interconnecting vessels between small arteries and veins or by removing the capillary network altogether and having two separate pumps pushing blood-like liquid through the arterial and venous system.

Nerves are exposed to combinations of tensile, shear and compressive *stresses* that result in nerve excursion and strain during joint movement (Topp & Boyd, 2012). Their structural organisation enables them to continue to function under these *stresses*. Nerves are composed of fascicles or bundles of axons encased within perineurium (modified ECM), with each individual axon encased in endoneurium. The fascicles are then covered externally by an epineurium, a denser layer of connective tissue. The endoneurium, perineurium and epineurium all contain varying types of collagen fibrils and other ECM components. It is thought that the elasticity and strength of nerve tissue is retained as long as the perineurium is intact (Sunderland, 1965). As found in most soft tissues, there is an initial toe region of the *stress–strain* curve which exhibits a low stiffness, followed by gradually increasing stiffness as the strain increases. When a nerve is subjected to an increasing tensile load, the elongation is proportional to the load until a certain point is reached, after which proportionality no longer holds. This point represents the elastic limit of the nerve beyond which the nerve passes into a semi-plastic state (Sunderland, 1965). One study conducted on rabbit peripheral nerves found that the linear stiffness was reached at about 20% *tensile strain* and that the slope of the *stress–strain* curve remained unchanged until failure (Rydevik et al. 1990). Nerve compliance is affected by anatomical position (Table 7). This is seen with experiments on the median and sciatic nerve which display more strain and less stiffness in the segments that cross the elbow and the hip than in their distal segments (Phillips et al. 2004). Minor reversible changes in peak nerve conduction velocity were found to occur in rabbit sciatic nerve at 8% *strain*, whereas gradual and irreversible changes occurred at 16.1% *strain* (Driscoll et al. 2002). Nerves are often a protected structure in surgical procedures and hence replicating their exact physical properties may be less critical in printing of complex multimaterial replicas of human body regions. In other words, if a surgeon's aim is to avoid cutting them, then they need not necessarily conform exactly to their natural state; however, their mechanical influence is important in terms of level of allowed tissue retraction. Even though they are a protected structure intra-operatively, it is not uncommon for them to display some element of neuropraxia postoperatively. This phenomenon would be difficult to replicate in a 3D print. In some procedures, such as thyroidectomies, nerves are identified using a nerve-monitoring system such as the Medtronic NIM (Medtronic PLC, Dublin, Ireland). Creating a 3D printed material that both conducts electricity and is sensitive to nearby diathermy or tension would allow for better surgical simulation. Pressure-sensing materials used in electronic skin devices could yield a possible solution. These are elastic, micro-structured conducting polymer thin films with ultra-sensitive resistive pressure sensors (Pan et al. 2014). Here, a polypyrrole hydrogel is used to prepare an elastic micro-structured conducting polymer/film which then has electrodes attached to it. Whether this is a technology that can be 3D printed and integrated into a model remains to be seen.

Conclusions

Due to many components affecting the *modulus of elasticity* in each bodily tissue, replication of their properties in 3D anatomical replicas would most likely require mimicking the contribution of each of the components. This task is made more difficult by the fact that much of the weight of most of these tissues is attributed to water. Current 3D printing technologies do not incorporate fluid into their 3D prints. With regard to creating anatomical prints that could serve as practice models for surgical training, one big hurdle that exists is finding a material that both matches the properties of the tissues involved in the operation and is also safe to dissect with diathermy. Much work has been done in tissue engineering to create tissue scaffolds that are both biocompatible and could serve as a reliable structural support until cells have grown into the scaffold. This work may aid in discovering materials that could serve in the creation of dissectible anatomy teaching or surgical simulation tools. For 3D prints to become a viable teaching option in surgical training they also need to be cost-effective. In other words, not only do the prints need to be cheaper than their donor cadaver counterparts but the benefit accrued from having trainees who are more confident and thorough in their operative technique afforded by the 3D prints needs to outweigh the cost of purchasing the print. The challenges faced in creating realistic anatomical prints are many and, due to the complexity within each tissue, each will most likely need to be represented by its own (composite) material, which would require a multimodal printer. Printing with hydrogel-like materials may move us a step closer towards having models that both feel and deform like real human tissue. Therefore, despite the rapid pace of change in 3D printing, much work still needs to be done to ascertain exactly which aspects are necessary to create effective surgical simulators using 3D printing.

Author contributions

Dr Ratheesraj Ratinam: acquisition of data, data analysis and interpretation, contribution to concept/design, drafting of the manuscript. Ms Michelle Quayle: critical revision of manuscript. Dr Michelle Lazarus: contribution to concept/design, critical revision of manuscript. Mr John Crock: critical revision of manuscript. Associate Professor Quentin A. Fogg: contribution to concept/design, critical revision of manuscript. Professor Paul G. McMenamin: contribution to concept/design, critical revision of manuscript.

References

3D Systems Corp. 2017a. Materials [Online]. Available: https://au.3dsystems.com/materials [accessed 1 December 2017].

3D Systems Corp. 2017b. *MultiJet Plastic Printers* [Online]. Available: https://au.3dsystems.com/sites/default/files/2017-03/3D-Systems_ProJet_MJP_3600_Plastic_SpecSheet_A4_US_2017.03.22_WEB_0.pdf [accessed 1 December 2017].

Abouhashem Y, Dayal M, Serafin S, et al. (2017) Students' attitudes toward body image donation for 3D printing. *Clin Anat* **30**, 1005–1006.

Ahima RS, Flier JS (2000) Adipose tissue as an endocrine organ. *Trends Endocrinol Metab* **11**, 327–332.

Albert CI, Jameson J, Harris G (2013) Design and validation of bending test method for characterization of miniature pediatric cortical bone specimens. *Proc Inst Mech Eng H* **227**, 105–113.

Alexander H, Cook T (1977) Accounting for natural tension in the mechanical testing of human skin. *J Invest Dermatol* **69**, 310–314.

Alkhouli N, Mansfield J, Green E, et al. (2013) The mechanical properties of human adipose tissues and their relationships to the structure and composition of the extracellular matrix. *Am J Physiol Endocrinol Metab* **305**, E1427–E1435.

Arvier J, Barker T, Yau Y, et al. (1994) Maxillofacial biomodelling. *Br J Oral Maxillofac Surg* **32**, 276–283.

Aslan M, Kenneth S, Hod L (2017) Soft material for soft actuators. *Nat Commun* **8**, 1–8.

ASM International (2002) *Atlas of Stress-Strain Curves*. 2nd edn. Materials Park, OH: ASM International.

Atkins T, Escudier M (2013) *A Dictionary of Mechanical Engineering*, 1st edn. Oxford: Oxford University Press.

Azizi E, Halenda GM, Roberts TJ (2009) Mechanical properties of the gastrocnemius aponeurosis in wild turkeys. *Integr Comp Biol* **49**, 51–58.

Benet A, Plata-Bello J, Abla AA, et al. (2015) Implantation of 3D-printed patient-specific aneurysm models into cadaveric specimens: a new training paradigm to allow for improvements in cerebrovascular surgery and research. *Biomed Res Int* **2015**, 939387.

Berman B (2012) 3-D printing: the new industrial revolution. *Bus Horiz* **55**, 155–162.

Berry E, Brown J, Connell M, et al. (1997) Preliminary experience with medical applications of rapid prototyping by selective laser sintering. *Med Eng Phys* **19**, 90–96.

Bollet AJ, Handy JR, Sturgill BC (1963) Chondroitin sulfate concentration and protein-polysaccharide composition of articular cartilage in osteoarthritis. *J Clin Invest* **42**, 853.

Boyer G, Molimard J, Tkaya MB, et al. (2013) Assessment of the in-plane biomechanical properties of human skin using a finite element model updating approach combined with an optical full-field measurement on a new tensile device. *J Mech Behav Biomed Mater* **27**, 273–282.

Bradway JK, Amadio PC, Cooney WP (1989) Open reduction and internal fixation of displaced, comminuted intra-articular fractures of the distal end of the radius. *J Bone Joint Surg Am* **71**, 839–847.

Burghardt AJ, Link TM, Majumdar S (2011) High-resolution computed tomography for clinical imaging of bone microarchitecture. *Clin Orthop Relat Res*, **469**, 2179–2193.

Bursać PM, Obitz TW, Eisenberg SR, et al. (1999) Confined and unconfined stress relaxation of cartilage: appropriateness of a transversely isotropic analysis. *J Biomech* **32**, 1125–1130.

Butscher A, Bohner M, Hofmann S, et al. (2011) Structural and material approaches to bone tissue engineering in powder-based three-dimensional printing. *Acta Biomater* **7**, 907–920.

Chang PS-H, Parker TH, Patrick CW Jr, et al. (2003) The accuracy of stereolithography in planning craniofacial bone replacement. *J Craniofac Surg* **14**, 164–170.

Claes E, Atienza J, Guinea G, et al. (2010) Mechanical properties of human coronary arteries. 2010 Annual International Conference of the IEEE Engineering in Medicine and Biology, 31 August – 4 September 2010. Buenos Aires: IEEE; 3792–3795.

Cohen J, Reyes SA (2015) Creation of a 3D printed temporal bone model from clinical CT data. *Am J Otolaryngol* **36**, 619–624.

Comninou M, Yannas IV (1976) Dependence of stress–strain nonlinearity of connective tissues on the geometry of collagen fibres. *J Biomech* **9**, 427–433.

Currey JD (1988) The effect of porosity and mineral content on the Young's modulus of elasticity of compact bone. *J Biomech* **21**, 131–139.

Currey JD (2004) Tensile yield in compact bone is determined by strain, post-yield behaviour by mineral content. *J Biomech* **37**, 549–556.

Diamant J, Keller A, Baer E, et al. (1972) Collagen; ultrastructure and its relation to mechanical properties as a function of ageing. *Proc R Soc Lond B Biol Sci* **180**, 293–315.

Diridollou S, Patat F, Gens F, et al. (2000) *In vivo* model of the mechanical properties of the human skin under suction. *Skin Res Technol* **6**, 214–221.

Driscoll PJ, Glasby MA, Lawson GM (2002) An *in vivo* study of peripheral nerves in continuity: biomechanical and physiological responses to elongation. *J Orthop Res* **20**, 370–375.

Drury JL, Mooney DJ (2003) Hydrogels for tissue engineering: scaffold design variables and applications. *Biomaterials* **24**, 4337–4351.

Duncan JM, Nahas S, Akhtar K, et al. (2015) The use of a 3D printer in pre-operative planning for a patient requiring acetabular reconstructive surgery. *J Orthop Case Rep* **5**, 23–25.

Flahiff CM, Gober GA, Nicholas RW (1995) Pullout strength of fixation screws from polymethylmethacrylate bone cement. *Biomaterials* **16**, 533–536.

Flügge W (1975) Viscoelasticity, 2nd edn., p. 3. Berlin.

Fung YC (1967) Elasticity of soft tissues in simple elongation. *Am J Physiol* **213**, 1532.

Gibson I, Rosen D, Stucker B (2014) *Additive Manufacturing Technologies: 3D Printing, Rapid Prototyping, and Direct Digital Manufacturing*. New York: Springer.

Giovinco NA, Dunn SP, Dowling L, et al. (2012) A novel combination of printed 3-dimensional anatomic templates and computer-assisted surgical simulation for virtual preoperative planning in Charcot foot reconstruction. *J Foot Ankle Surg* **51**, 387–393.

Hariri HH, Schlenoff JB (2010) Saloplastic macroporous polyelectrolyte complexes: cartilage mimics. *Macromolecules* **43**, 8656–8663.

Hochman JB, Kraut J, Kazmerik K, et al. (2013) Generation of a 3D printed temporal bone model with internal fidelity and validation of the mechanical construct. *Otolaryngol Head Neck Surg* **150**, 448–454.

Hochman JB, Rhodes C, Kraut J, et al. (2015a) End user comparison of anatomically matched 3-dimensional printed and virtual haptic temporal bone simulation: a pilot study. *Otolaryngol Head Neck Surg* **153**, 263–268.

Hochman JB, Rhodes C, Wong D, et al. (2015b) Comparison of cadaveric and isomorphic three-dimensional printed models in temporal bone education. *Laryngoscope* **125**, 2353–2357.

Holeček M, Kochová P, Tonar Z (2011) Mechanical properties of living cells and tissues related to thermodynamics, experiments and quantitative morphology-a review. *IntechOpen*, 3–20.

Holzapfel GA (2001) Biomechanics of soft tissue. *Handb Mat Behav Models* **3**, 1049–1063.

Honiball JR (2010) *The Application of 3D Printing in Reconstructive Surgery*. Stellenbosch: University of Stellenbosch.

Hopper TAJ (2005) *Quantitative MRI and Micro-CT of Bone Architecture: Applications and Limitations in Orthopaedics*. Brisbane: Queensland University of Technology.

Hori RY, Mockros L (1976) Indentation tests of human articular cartilage. *J Biomech* **9**, 259–268.

Horvath JC (2014) *Mastering 3D Printing*. Berkeley, CA: Apress.

Huang H, Hsieh MF, Zhang G, et al. (2015) Improved accuracy of 3D-printed navigational template during complicated tibial plateau fracture surgery. *Australas Phys Eng Sci Med* **38**, 109–117.

Humphrey JD, Rourke SL (2015) *An Introduction to Biomechanics: Solids and Fluids, Analysis and Design*, 2nd edn. New York, NY: Springer.

Imer R, Akiyama TF, de Rooij N, et al. (2009) The measurement of biomechanical properties of porcine articular cartilage using atomic force microscopy. *Arch Histol Cytol* **72**, 251–259.

Jacobs S, Grunert R, Mohr FW, et al. (2008) 3D-Imaging of cardiac structures using 3D heart models for planning in heart surgery: a preliminary study. *Interact Cardiovasc Thorac Surg* **7**, 6–9.

Khuri J, Wertheimer S, Krueger J, et al. (2003) Fixation of the offset V osteotomy: mechanical testing of 4 constructs. *J Foot Ankle Surg* **42**, 63–67.

Kirk RM (2010) *Basic Surgical Techniques*. New York: Churchill Livingstone/Elsevier.

Klein GT, Lu Y, Wang MY (2013) 3D printing and neurosurgery —ready for prime time? *World Neurosurg* **80**, 233–235.

Knirk JL, Jupiter JB (1986) Intra-articular fractures of the distal end of the radius in young adults. *J Bone Joint Surg Am* **68**, 647–659.

Kobayashi H, Kawamoto S, Brechbiel MW, et al. (2004) Micro-MRI methods to detect renal cysts in mice. *Kidney Int* **65**, 1511–1516.

Korhonen RK, Saarakkala S (2011) Biomechanics and modeling of skeletal soft tissues. In: *Theoretical Biomechanics*. (ed. Klika V), pp. 113–132, Croatia: InTech Europe.

Korhonen R, Laasanen M, Töyräs J, et al. (2002) Comparison of the equilibrium response of articular cartilage in unconfined compression, confined compression and indentation. *J Biomech* **35**, 903–909.

Krasiński Z, Biskupski P, Kaczmarek E, et al. (2010) The influence of elastic components of the venous wall on the biomechanical properties of different veins used for arterial reconstruction. *Eur J Vasc Endovasc Surg* **40**, 224–229.

Krishnan S, Dawood A, Richards R, et al. (2012) A review of rapid prototyped surgical guides for patient-specific total knee replacement. *J Bone Joint Surg Br* **94**, 1457–1461.

Kumbar S, Laurencin CT, Deng M (2014) *Natural and Synthetic Biomedical Polymers*. Boston: Elsevier Science.

Kurenov SN, Ionita C, Sammons D, et al. (2015) Three-dimensional printing to facilitate anatomic study, device development, simulation, and planning in thoracic surgery. *J Thorac Cardiovasc Surg* **149**, 973–979. e1

Lackey DE, Burk DH, Ali MR, et al. (2014) Contributions of adipose tissue architectural and tensile properties toward

defining healthy and unhealthy obesity. *Am J Physiol Endocrinol Metab* **306**, E233.

LaCourse JR, Vogt M, Miller W, et al. (1988) Spectral analysis interpretation of electro-surgical generator nerve and muscle stimulation. *IEEE Trans Biomed Eng* **35**, 505–509.

Lakes RS (2009) *Viscoelastic Materials*. New York, NY: Cambridge University Press.

Lam K (1985) Simultaneous handling of the diathermy pen and scalpel. *Laryngoscope* **95**, 348–348.

Lardner TJ (1994) *Mechanics of Solids: An Introduction*. New York, NY: McGraw-Hill.

Laurencin CT, Freeman JW (2005) Ligament tissue engineering: an evolutionary materials science approach. *Biomaterials* **26**, 7530–7536.

Li WC, Ruan XZ, Zhang HM, et al. (2006) Biomechanical properties of different segments of human umbilical cord vein and its value for clinical application. *J Biomed Mater Res B* **76**, 93–97.

Li S, Demirci E, Silberschmidt VV (2013) Variability and anisotropy of mechanical behavior of cortical bone in tension and compression. *J Mech Behav Biomed Mater* **21**, 109–120.

Lieber RL, Runesson E, Einarsson F, et al. (2003) Inferior mechanical properties of spastic muscle bundles due to hypertrophic but compromised extracellular matrix material. *Muscle Nerve* **28**, 464–471.

Liebschner MA (2004) Biomechanical considerations of animal models used in tissue engineering of bone. *Biomaterials* **25**, 1697–1714.

Lim KHA, Loo ZY, Goldie SJ, et al. (2016) Use of 3D printed models in medical education: a randomized control trial comparing 3D prints versus cadaveric materials for learning external cardiac anatomy. *Anat Sci Educ* **9**, 213–221.

Lipton JI, Tow AP, Burbank I, et al. (2014) Solid Freeform Fabrication of Soft Tissue Simulators for Needle Injection. Solid Freeform Fabrication Symposium, 2014 Austin, Texas. University of Texas, 2012.

Loukas M, Shoja MM, Thurston T, et al. (2008) Anatomy and biomechanics of the vertebral aponeurosis part of the posterior layer of the thoracolumbar fascia. *Surg Radiol Anat* **30**, 125–129.

Lubliner JA (2014) *Introduction to Solid Mechanics: An Integrated Approach*. New York: Springer.

Ma Z, Hu S, Tan JS, et al. (2013) *In vitro* and *in vivo* mechanical properties of human ulnar and median nerves. *J Biomed Mater Res A* **101**, 2718–2725.

Maganaris CN (2002) Tensile properties of *in vivo* human tendinous tissue. *J Biomech* **35**, 1019–1027.

Mahaisavariya B, Sitthiseripratip K, Oris P, et al. (2006) Rapid prototyping model for surgical planning of corrective osteotomy for cubitus varus: report of two cases. *Injury Extra* **37**, 176–180.

Matschke V, Jones JG, Lemmey AB, et al. (2013) Patellar tendon properties and lower limb function in rheumatoid arthritis and ankylosing spondylitis versus healthy controls: a cross-sectional study. *ScientificWorldJournal* **2013**, 1–8.

Matsuhashi T, Hooke AW, Zhao KD, et al. (2014) Tensile properties of a morphologically split supraspinatus tendon. *Clin Anat* **27**, 702–706.

Mayrovitz HN, Corbitt K, Grammenos A, et al. (2017) Skin indentation firmness and tissue dielectric constant assessed in face, neck, and arm skin of young healthy women. *Skin Res Technol* **23**, 112–120.

McBride DJ, Trelstad RL, Silver FH (1988) Structural and mechanical assessment of developing chick tendon. *Int J Biol Macromol* **10**, 194–200.

McVeigh GE, Bank AJ, Cohn JN (2007) Arterial compliance. In: *Cardiovascular Medicine*. (eds Willerson JT, Wellens HJJ, Cohn JN, Holmes DR Jr), pp. 1811. London: Springer.

Melnikova R, Ehrmann A, Finsterbusch K (2014) 3D printing of textile-based structures by Fused Deposition Modelling (FDM) with different polymer materials. IOP Conference Series: Materials Science and Engineering, 2014. IOP Publishing, 012018.

Millesi H, Reihsner R, Hamilton G, et al. (1995) Biomechanical properties of normal tendons, normal palmar aponeuroses, and tissues from patients with Dupuytren's disease subjected to elastase and chondroitinase treatment. *Clin Biomech Elsevier Ltd* **10**, 29–35.

Mori K, Yamamoto T, Nakao Y, et al. (2010) Development of artificial cranial base model with soft tissues for practical education: technical note. *Opera Neurosurg* **66**, onsE339–onsE341.

Morrow DA, Donahue TLH, Odegard GM, et al. (2010) Transversely isotropic tensile material properties of skeletal muscle tissue. *J Mech Behav Biomed Mater* **3**, 124–129.

Mosler E, Folkhard W, Knörzer E, et al. (1985) Stress-induced molecular rearrangement in tendon collagen. *J Mol Biol* **182**, 589–596.

Mow VC, Holmes MH, Lai WM (1984) Fluid transport and mechanical properties of articular cartilage: a review. *J Biomech* **17**, 377–394.

Mowry SE, Jammal H, Myer C IV, et al. (2015) A novel temporal bone simulation model using 3D printing techniques. *Otol Neurotol* **36**, 1562–1565.

Mozersky D, Sumnfr D, Hokanson D, et al. (1972) Transcutaneous measurement of the elastic properties of the human femoral artery. *Circulation* **46**, 948–955.

Murphy SV, Atala A (2014) 3D bioprinting of tissues and organs. *Nat Biotechnol* **32**, 773–785.

Neuman RE, Logan MA (1950) The determination of collagen and elastin in tissues. *J Biol Chem* **186**, 549–556.

Olivieri LJ, Su L, Hynes CF, et al. (2016) 'Just-In-Time' simulation training using 3-D printed cardiac models after congenital cardiac surgery. *World J Pediatr Congenit Heart Surg* **7**, 164–168.

Ottenio M, Tran D, Annaidh AN, et al. (2015) Strain rate and anisotropy effects on the tensile failure characteristics of human skin. *J Mech Behav Biomed Mater* **41**, 241–250.

Pan L, Chortos A, Yu G, et al. (2014) An ultra-sensitive resistive pressure sensor based on hollow-sphere microstructure induced elasticity in conducting polymer film. *Nat Commun* **5**, 1–8.

Pei E (2014) 4D printing: dawn of an emerging technology cycle. *Assemb Autom* **34**, 310–314.

Petzold R, Zeilhofer HF, Kalender WA (1999) Rapid prototyping technology in medicine – basics and applications. *Comput Med Imaging Graph* **23**, 277–284.

Phillips JB, Smit X, Zoysa ND, et al. (2004) Peripheral nerves in the rat exhibit localized heterogeneity of tensile properties during limb movement. *J Physiol* **557**, 879–887.

Pigazzi A, Hellan M, Ewing DR, et al. (2007) Laparoscopic medial-to-lateral colon dissection: how and why. *J Gastrointest Surg* **11**, 778.

Poole WE, Marsland D, Durani P, et al. (2016) Detecting dorsal screw penetration following volar plate fixation of the distal

radius – A validation study in a saw bone model. *Trauma* **19**, 46–53.

Potamianos P, Amis A, Forester A, et al. (1998) Rapid prototyping for orthopaedic surgery. *Proc Inst Mech Eng H* **212**, 383–393.

Ratner BD, Hoffman AS (1976) Synthetic hydrogels for biomedical applications. *Hydro Med Relat Appl* **31**, 1–36.

Raub CB, Unruh J, Suresh V, et al. (2008) Image correlation spectroscopy of multiphoton images correlates with collagen mechanical properties. *Biophys J* **94**, 2361–2373.

Richter A (2009) Hydrogels for actuators. In: *Hydrogel Sensors and Actuators: Engineering and Technology*, (eds Arndt K-F, Gerlach G) pp. 221–248. Berlin: Springer.

Rose AS, Kimbell JS, Webster CE, et al. (2015a) Multi-material 3D models for temporal bone surgical simulation. *Ann Otol Rhinol Laryngol* **124**, 528–536.

Rose AS, Webster CE, Harrysson OL, et al. (2015b) Pre-operative simulation of pediatric mastoid surgery with 3D-printed temporal bone models. *Int J Pediatr Otorhinolaryngol* **79**, 740–744.

Rossmann JS (2010) Elastomechanical properties of bovine veins. *J Mech Behav Biomed Mater* **3**, 210–215.

Roylance D (2001) *Stress-Strain Curves* [Online]. Cambridge, MA: Massachusetts Institute of Technology. Available: https://ocw.mit.edu/courses/materials-science-and-engineering/3-11-mechanics-of-materials-fall-1999/modules/MIT3_11F99_ss.pdf [accessed 1 December 2017].

Ryan JR, Chen T, Nakaji P, et al. (2015) Ventriculostomy simulation using patient-specific ventricular anatomy, 3D printing, and hydrogel casting. *World Neurosurg* **84**, 1333–1339.

Ryan JR, Almefty KK, Nakaji P, et al. (2016) Cerebral aneurysm clipping surgery simulation using patient-specific 3D printing and silicone casting. *World Neurosurg* **88**, 175–181.

Rydevik BL, Kwan MK, Myers RR, et al. (1990) An *in vitro* mechanical and histological study of acute stretching on rabbit tibial nerve. *J Orthop Res* **8**, 694–701.

Sanders R (1973) Torsional elasticity of human skin *in vivo*. *Pflügers Arch Eur J Physiol* **342**, 255–260.

Sangian D, Jeiranikhameneh A, Naficy S, et al. (2018) Three-dimensional printed braided sleeves for manufacturing McKibben artificial muscles. 3D Printing and Additive Manufacturing [Online]. Available: https://www.liebertpub.com/doi/abs/10.1089/3dp.2018.0103 [accessed 8 November 2018].

Saran BR, Brucker AJ, Maguire AM (1994) Drainage of subretinal fluid in retinal detachment surgery with the El-Mofty insulated diathermy electrode. *Retina* **14**, 344–347.

Scawn RL, Foster A, Lee BW, et al. (2015) Customised 3D printing: an innovative training tool for the next generation of orbital surgeons. *Orbit* **34**, 216–219.

Schmauss D, Haeberle S, Hagl C, et al. (2015) Three-dimensional printing in cardiac surgery and interventional cardiology: a single-centre experience. *Eur J Cardiothorac Surg* **47**, 1044–1052.

Segal Y, Gotlieb W, Ben-Baruch G (1997) Intra-operative use of the loop diathermy for liver biopsies during gynecologic surgery. *Int J Gynecol Cancer* **7**, 477–479.

Seitz H, Tille C, Irsen S, et al. (2004) Rapid Prototyping models for surgical planning with hard and soft tissue representation. *Int Congr Ser* **1268**, 567–572.

Sengupta S, Webb DR (2001) Use of a computer-controlled bipolar diathermy system in radical prostatectomies and other open urological surgery. *ANZ J Surg* **71**, 538–540.

Shaw MT (2005) *Introduction to Polymer Viscoelasticity*. Hoboken, NJ: Wiley-Interscience.

Singare S, Lian Q, Ping Wang W, et al. (2009) Rapid prototyping assisted surgery planning and custom implant design. *Rapid Prototyp J* **15**, 19–23.

Souzaki R, Kinoshita Y, Ieiri S, et al. (2015) Preoperative surgical simulation of laparoscopic adrenalectomy for neuroblastoma using a three-dimensional printed model based on preoperative CT images. *J Pediatr Surg* **50**, 2112–2115.

Stenquist BC, Holt PJ, Motley RJ (2002) Computerized bipolar diathermy with scissors and forceps in cutaneous surgery. *Dermatol Surg* **28**, 601–602.

Stratasys Ltd. (2014) Polyjet Materials Data Sheet [Online]. Available: http://usglobalimages.stratasys.com/Main/Files/Material_Spec_Sheets/MSS_PJ_PJMaterialsDataSheet.pdf?v=635785205440671440 [accessed 20 May 2017].

Stratasys Ltd. (2017a) CONNEX3 OBJET260 [Online]. Available: http://www.stratasys.com/3d-printers/objet260-connex3 [accessed 1 December 2017].

Stratasys Ltd. (2017b) Materials by Technology: Stereolithography [Online]. Available: www.stratasysdirect.com/materials/stereolithography [accessed 1 December 2017].

Stratasys Ltd. (2017c) Our materials [Online]. Available: www.stratasys.com/materials/search [accessed 1 December 2017].

Sunderland S (1965) The connective tissues of peripheral nerves. *Brain* **88**, 841–854.

Sunderland S, Bradley K (1961a) Stress-strain phenomena in human peripheral nerve trunks. *Brain* **84**, 102–119.

Sunderland S, Bradley KC (1961b) Stress-strain phenomena in denervated peripheral nerve trunks. *Brain* **84**, 125–127.

SYNBONE. (2017) *Studentenforum-SYNBONE. 134*. Munich: Kongress Deutsche Gesellschaft fur Chirurgie.

Tai BL, Wang AC, Joseph JR, et al. (2016) A physical simulator for endoscopic endonasal drilling techniques: technical note. *J Neurosurg* **124**, 811–816.

Tam MD, Laycock SD, Bell DG, et al. (2012) 3-D printout of a DICOM file to aid surgical planning in a 6 year old patient with a large scapular osteochondroma complicating congenital diaphyseal aclasia. *J Radiol Case Rep* **6**, 31–37.

Tanaka T, Nishio I, Sun S-T, et al. (1982) Collapse of gels in an electric field. *Science* **218**, 467–469.

Topp KS, Boyd BS (2012) Peripheral nerve: from the microscopic functional unit of the axon to the biomechanically loaded macroscopic structure. *J Hand Ther* **25**, 142–152.

Ugbolue UC, Gislason MK, Carter M, et al. (2015) Tensile properties of the transverse carpal ligament and carpal tunnel complex. *Clin Biomech Elsevier Ltd* **30**, 649–656.

Ussmueller JO, Jaehne M, Neumann B-G (2004) The use of diathermy scissors in parotid gland surgery. *Arch Otolaryngol Head Neck Surg* **130**, 187–189.

Vakharia VN, Vakharia NN, Hill CS (2016) Review of 3-dimensional printing on cranial neurosurgery simulation training. *World Neurosurg* **88**, 188–198.

Van Loocke M, Simms C, Lyons C (2009) Viscoelastic properties of passive skeletal muscle in compression-cyclic behaviour. *J Biomech* **42**, 1038–1048.

Vignos PJ Jr, Lefkowitz M (1959) A biochemical study of certain skeletal muscle constituents in human progressive muscular dystrophy. *J Clin Invest* **38**, 873.

Vorp DA, Schiro BJ, Ehrlich MP, et al. (2003) Effect of aneurysm on the tensile strength and biomechanical behavior of the ascending thoracic aorta. *Ann Thorac Surg* **75**, 1210–1214.

Wain R, Rimouche S, Srinivasan J (2010) Controlled muscle division during flap surgery: a simple technique. *Eur J Plast Surg* **33**, 295–296.

Weisman J, Tappa K, Nicholson J, et al. (2015) 3D printing antibiotic and chemotherapeutic eluting catheters and constructs. *J Vasc Interv Radiol* **2**, S12.

Zein NN, Hanouneh IA, Bishop PD, et al. (2013) Three-dimensional print of a liver for preoperative planning in living donor liver transplantation. *Liver Transpl* **19**, 1304–1310.

Supporting Information

Additional Supporting Information may be found in the online version of this article:

Appendix S1. Biomechanics terminology.